Characterization of Flow Regime Transition and Particle Motion Using Acoustic Emission Measurement in a Gas-Solid Fluidized Bed

Wang Jingdai, Ren Congjing, and Yang Yongrong
State Key Laboratory of Chemical Engineering, Dept. of Chemical and Biochemical Engineering, Zhejiang University, Hangzhou 310027, People's Republic of China

DOI 10.1002/aic.12071
Published online October 23, 2009 in Wiley InterScience (www.interscience.wiley.com).

Particle motion is a major determinant of the dynamical performance of a fluidized bed. It plays an important role in determining and optimizing the complex correlation of fluidization condition between particle-particle and particle-environment in a system. A passive acoustic emission (AE) technique is applied to monitor, characterize, and control the fluidization condition of polyethylene particles in a gas-solid fluidized bed. Experimental results show that AE signals are very sensitive to the particle movements by analyzing energy distribution, which can help to understand the status of the system. The AE energy temporal analysis is further used to identify the transition of flow regimes. Moreover, the activity of particle motion can be quantitatively determined by using a combination of granular temperature and AE spatial energy analysis. This work provides valuable insights into the dynamic behavior of particles in a gas-solid fluidized bed based on AE technique. © 2009 American Institute of Chemical Engineers *AIChE J,* 56: 1173–1183, 2010
Keywords: fluidized bed, flow regime, particle motion, acoustic emission, energy analysis, measurement

Introduction

Fluidized beds are widely used in the chemical industry, not only because of its excellent mixing ability, but also its efficient heat- and mass-transfer rates. The stable operation of a gas-solid fluidized bed at a specific fluid-dynamic state is important for the control of flow regimes and fluidization condition. Hence, the understanding of fluid-dynamic behavior in the bed is critical for rational design of the fluidized bed and optimization of operating conditions. However, it is a very challenging task to control fluidization conditions for a conventional fluidized bed due to its invisible access to the inner bed.

Fluidization regimes can be characterized and determined by fluidization states of the bed, which have typical common features independent of change of operating conditions. The fluidization state can be characterized and quantified by analyzing parameters such as the minimum fluidization velocity (U_{mf}), and the onset of turbulent fluidization (U_c). Numerous studies have been conducted to investigate U_{mf} and U_c by using pressure gradient and pressure fluctuation methods.[1–7] Davidson and Harrison[1] developed the classical U_{mf} method to determine the fluid-dynamic behavior. After that, Wen and Yu[2] proposed a semi-empirical formula to calculate U_{mf} using various particles of size. Alternatively, pressure gradient method[3-7] is widely used to determine U_{mf}, evaluate the onset of turbulent fluidization, and characterize the transition from bubbling to turbulent regimes in fluidized beds due to its intuitivistics and simplicity. However, the pressure gradient method suffers from disrupting pressure fluctuation responsive to gas velocity, especially for adhesive powder and fines systems, leading to the difficulty in the determination of U_{mf} and U_c.

Correspondence concerning this article should be addressed to W. Jingdai at wangjd@zju.edu.cn

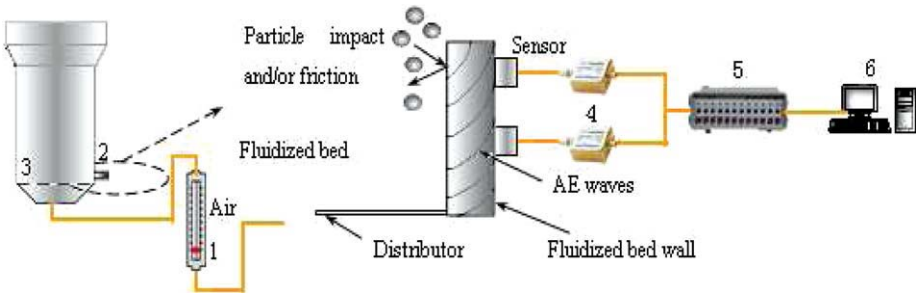

Figure 1. Schematic diagram of experimental apparatus.

(1) Orifice flow meter; (2) AE sensor; (3) distributor; (4) preamplifier; (5) signal conditioning; (6) computer. [Color figure can be viewed in the online issue, which is available at www.interscience.wiley.com.]

On the other hand, it is commonly accepted that the stable run of the fluidized bed is very important in the industrial processes.[8-9] Stable operation can be achieved by controlling particle behaviors including the enhancement of particle mixing and motion, and the prevention of particle sintering and agglomeration. Many conventional methods using electrostatic,[10-11] pressure,[12-13] temperature, radiation and optic measurements[14] have been used to control stable fluidization state. However, it is very difficult to detect early the occurrence of particle sintering and agglomeration, because of its slow aggregation and heterogeneous size using the aforementioned conventional methods. For instance, the temperature and pressure signals are not sensitive to the defluidized status,[13-18] radiation technique is harmful to the human health, and optical method is only effective to the regions close to the sensor and is not suitable to the rigorous fluidized conditions in a realistic plant. Hence, it is important to find a new technique, which can effectively and detect early the unstable state prior to defluidization.

Comparing with the other methods addressed previously, passive AE signals provide affluent information about the size and movement of fluidized particles. Since particle frictions and collisions generate AE waves, the hydrodynamics in fluidized beds such as particle flow velocity, type of flow, and fluidization condition in the bed can be detected by analyzing the time series of the signals. In other words, AE signal is *sensitive* and *selective* to the movement of the particles. Many recent publications on the applications[19-26] of AE measurement indicate that they lead to reliable quantitative results and do not function just as qualitative indicators, as was the case in the beginning phases of AE-based applications in nondestructive testing.[19] In this work, we for the first time developed and applied a passive acoustic emission (AE) technique, to investigate the flow regime and fluidization condition of polyethylene particles in a gas-solid fluidized bed. The relationship between AE temporal energy distribution and flow regimes was obtained. Furthermore, we proposed a model to describe the activity of particle motion in different regions by combining the granular temperature and AE spatial energy analysis. This work provides valuable insights into the dynamic behavior of particles in the fluidized system.

Experimental apparatus

Figure 1 is a schematic diagram of the experimental apparatus used in this study. It consisted of two parts: a fluidized bed and the acoustic emission measurement system.

The fluidized bed was made of transparent Plexiglas with an inside diameter of 250 mm, and a height of 3,000 mm. The fluidization status and particular behavior of bubbles and particles in the bed can be explicitly observed. The perforated-plate distributor with pore diameter of 2.0 mm, and an open area ratio of 2.6% was installed at the bottom. Compressed air was provided at the bottom to facilitate pneumatic transport of the particulate materials. The superficial gas velocity was controlled within 0 to 1.1 $m \cdot s^{-1}$. LLDPE particles (SINOPEC) with different average sizes were used in the experiments, including 0.306, 0.482, 0.522, 0.584, 0.640 and 0.820 mm. The density of particles is 944 $kg \cdot m^{-3}$. The particles were classified as Geldart B group. The height of the fixed bed was 800 mm.

The acoustic shot noise online collection and analysis system was developed by UNILAB Research Center of Chemical Engineering in Zhejiang University. It consisted of the data collection system and the computer. The data collection system included AE signal sensor, amplifier and A/D conversion. AE sensor used in this study was piezoelectric accelerometer with resonance frequency of 100-kHz, which is widely used in collecting the acceleration of vibration without the noise transferred via the air (PXR 15, 50 – 250 kHz, 150 dB). The sensor was mounted at special locations with silicone. The sampling frequency was 500 kHz, and the sampling time was 5 s.

In this work, AE was the mechanical energy released in the form of characteristic mechanical vibrations.[21] Piezoelectric devices can easily detect these characteristic waveforms. As is shown in Figure 1, AE waves generating in the fluidized in the bed can be sampled by the AE sensor. The signals pass through the amplifier and then pressure signals were converted to electric signals by A/D conversion. Finally, electric data was collected automatically by computer.

Results and Analysis

Temporal distribution of AE average energy and transition of flow regimes

Selection of AE Sensor Location. As discussed previously, AE signals provide abundant information of particle movement and can reflect the fluidization status in bed. Appropriate location for AE sensor is also important to the result. In the process of particle fluidization, gas bubbles are formed and developed gradually from the gas distributor, thus, the particles begin to move due to the interaction and

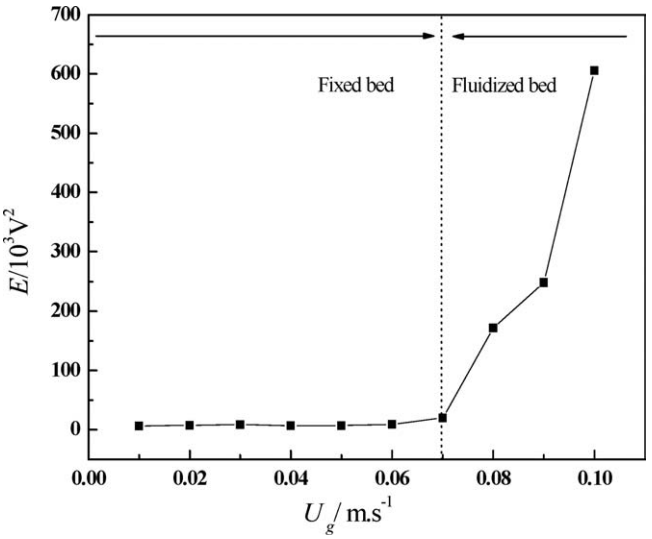

Figure 2. Relationship between average energy and velocity in small scale (Ug = 0.01–0.1 m·s^{-1}, dp = 0.482 mm).

coalescence of bubbles. The AE signals near the gas distributor are generated as a result of the interaction between particles and bubbles, so they indicate the change of particle motion in the first instance. In this experiment, the AE sensor was installed under the gas distributor to determine the flow regimes.

Temporal Energy Analysis of Signals. The AE time series collected by AE sensors are $[x_1, x_2, x_3 \ldots, x_N]$. Hence, the average energy of signals is defined as

$$E = \frac{\sum_{i=1}^{N} x_i^2}{N} \tag{1}$$

As the gas velocity varies from 0.01 to 1.0 m·s^{-1}, AE signals under different velocity were collected from the sensor mounted under the gas distributor. According to Eq. 1, the relationship between the average energy of signals and gas velocity can be obtained. Take the particles with $dp = 0.482$ mm as an example, Figure 2 shows the detail of AE energy at low-velocity scale ($U_g < 0.1$ m·s^{-1}). As shown in Figure 2, when the gas velocity is less than 0.07 m·s^{-1}, the average energy E changes little with gas velocity, and the amplitude maintains around 10 ($\times 10^3 V^2$). In general, the system is a fixed bed and not up to fluidization status when the gas velocity is less than U_{mf}. There are no practical acoustic emissions, because there is no movement of bed particles. Therefore, the average energy of signals measured in this region is only background noise from the equipment (E = 10 V^2). Once the gas velocity increases to above U_{mf}, the bed starts expansion. The "threshold point" from the fixed bed to the fluidized bed is the minimum fluidized velocity. Upon onset of fluidization at Ug = 0.07 m·s^{-1}, bubbles formed in the bed ($U_{mf} \approx U_{mb}$ for Geldart B particles) cause mild expansion, and the distributor gives consistent uniform flow with the formation of small bubbles evenly distributed symmetrically across it. Meanwhile, the average energy E increases significantly as the gas velocity U_g goes beyond 0.07 m·s^{-1}. The reason of the increase of E is considered to be the increase of the frequency and strength of the particle-particle and/or particle-distributor frictions and collisions. Hence, the "threshold point" at Ug = 0.07 m·s^{-1} indicates the transition of flow regime from the fixed bed to fluidized bed.

Figure 3 shows the correlation between E and U_g in large-scale gas velocity. It can be observed from Figure 3 that the average energy of AE signals maintains relative stable when the gas velocity is less than 0.31 m·s^{-1}. While beyond "turning point" at Ug = 0.31 m·s^{-1}, the average energy starts to increase rapidly with the gas velocity. In a fluidized bed, the coalescence and growth of bubbles and the breakup of bubbles are two opposite behaviors. At the beginning, when the gas velocity starts to increase, the average size of the bubbles increases with gas velocity in the process of fluidization. However, when the gas velocity reaches U_c, which equals to U_g at 0.31 m·s^{-1} in Figure 3, the trend of breakup of bubbles becomes more significant than that of coalescence and growth. Consequently, the population of larger bubbles gradually diminishes and the population of smaller bubbles increases. More bubbles cause more changes to the motion of particles in the bed, and increase the amplitude of AE energy. The emergence of abundant small bubbles promotes a high degree of mixing between the particles, and ensures that the particles are circulated throughout the bed. In this process, the transition of flow regime from the fluidized bed to the turbulent bed takes place. Likewise, the "turning point" of AE energy at Ug = 0.31 m·s^{-1} indicates this transition.

As previously illustrated, AE energy analysis is proved to be sensitive to the transition of flow regimes, which results in the sudden increase of energy amplitude at U_{mf} and U_c. The derivative of E with respect to superficial gas velocity R_E is defined as follows for more detailed analysis

$$R_E(j) = E_{j+1}/E_j \tag{2}$$

where j is the ordinal number of sample points from Ug = 0.01 m·s^{-1}.

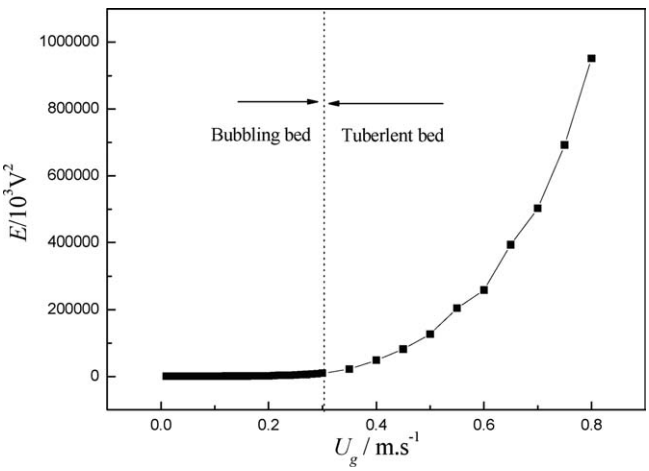

Figure 3. Relationship between average energy and velocity in big scale (Ug = 0.01–1.0 m·s^{-1}, dp = 0.482 mm).

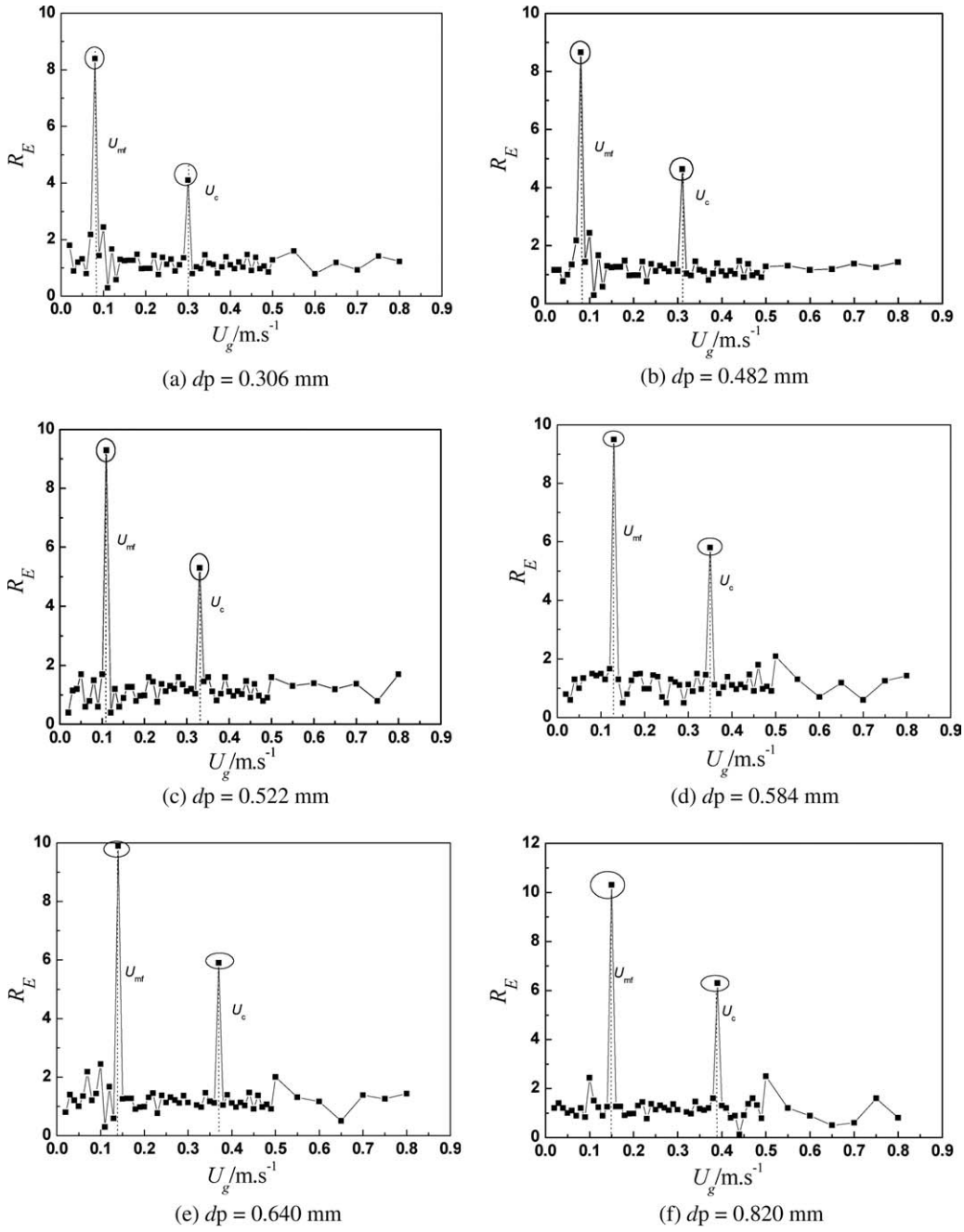

Figure 4. Relationship between R_E and U_g with different particle size: (a) dp = 0.306 mm; (b) dp = 0.482 mm; (c) dp = 0.522 mm; (d) dp = 0.584 mm; (e) dp = 0.640 mm; (f) dp = 0.820 mm.

In Figure 4b, the change of R_E of particle with dp = 0.482 mm is obtained as a function of gas velocity U_g. It can be observed that there are two obvious peaks in this figure, which means sudden increases of AE energy at these two "turning" points. The first peak occurs at Ug = 0.07 m·s^{-1}, and the value of R_E is approximately 9. The second peak occurs at Ug = 0.31 m·s^{-1} with R_E of 5. According to the aforementioned analysis, the bed starts to fluidize upon the gas velocity of 0.07 m·s^{-1}, and the flow regime turns to "turbulent" beyond the gas velocity of 0.31 m·s^{-1}. The value of R_E at Ug = 0.07 m·s^{-1} is larger than at Ug = 0.31 m·s^{-1}. This is possibly because that the AE sensor is more sensitive to the change of bubble behavior from nothing to a low level than the change from the low level to the high level.

According to the significant changes of AE energy as flow regime changes, a criterion to determine the flow regimes based on AE measurement is obtained. This can be presented as follows.

The derivative of AE energy R_E (dE/dv), is proposed and used to obtain the minimum fluidization velocity (the first peak in the curve of R_E vs. U_g), and the onset of turbulent

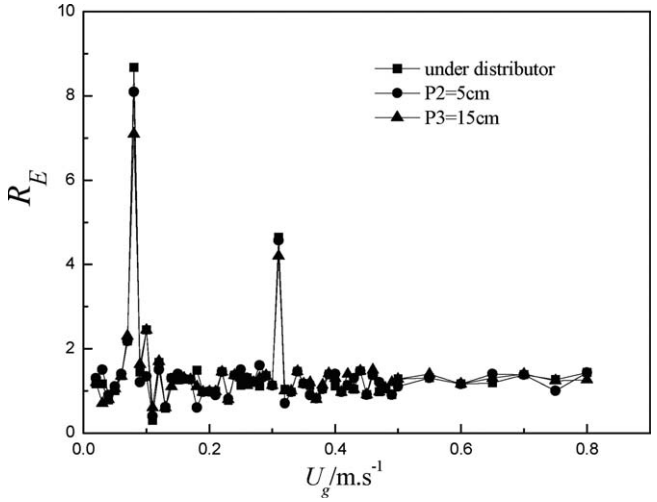

Figure 5. Relationship between R_E and U_g for different sensor locations (dp = 0.482 mm).

fluidization (the second of peak in the curve of R_E vs. U_g), in good agreement with the classic pressure gradient and fluctuation methods.

Effect of Particle Size on AE Average Energy. One particular issue of the criterion based on AE method is its adaptability when the particle size changes. Figure 4 shows the correlations between R_E and gas velocity U_g with different particle sizes. The data revealed that the relationship between R_E and U_g is consistent as particle size varies and all curves present two peaks at certain gas velocities (U_{mf} and U_c). As shown in Figure 4, the peak values increase with d_p, which we assume that the AE average energy is proportional to particle size under the same condition and sample properties such as particle density and particle shape. In this instance, the presumed criterion to determine the transition of flow regimes through AE energy analysis is suitable to particles with different sizes.

Effect of Sensor Location on AE Average Energy. It is necessary to address that a proper measurement place is of crucial importance to the effectiveness of this methodology. As the transition of flow regimes in the fluidized bed is essentially caused by bubble behavior, it is important to understand the bubble behavior in the bed. Figure 5 presents the results obtained from the AE sensors placed in various positions. One sensor was located under the distributor, and the other two were mounted on the outer wall of the bed with an axial height of 5 cm and 15 cm, respectively. As shown in Figure 5, the highest amplitude peaks appeared to be the sensor mounted under the gas distributor.

Under most fluidization conditions, the gas bubbles generate and grow up from the orifices of the gas distributor. The small bubbles that form at the bottom of the bed interact, causing larger bubbles to form. These larger bubbles lead to the particle movement; hence, the bubbles develop in the way of down-to-up. Accordingly, the particles in the bed move due to the motion of the bubble phase. This process is progressive with height and results in the distinct influence of sensor location on the AE energy. That is, the transition of flow regimes generally develops from down-to-up. On the other hand, the measurement applied in this study was done for vibration. According to acoustic theory, AE waves attenuate exponentially as they are propagating. So, the sensor mounted under the distributor is more sensitive to the change of particle motion, and can indicate the transition of flow regimes in the first stance.

Results of AE Measurement Compared with Other Methods. Furthermore, in order to check the veracity of the criterion, formulas and classic measurements (pressure gradient and fluctuation methods) have been estimated. The results listed in Figure 6 indicated that the results from the AE method are consistent with that from the formulas and classic method.

Spatial distribution of AE average energy and particle motion activity

Gas-solid fluidized bed is a system which involves extremely complicated interaction between particles-bubbles and particles-particles. For industrial applications with such processes, it is important to monitor and control the fluidization status to prevent the occurrence of defluidization, such as agglomeration and blocking. However, understanding of fluidization status is difficult for conventional fluidized bed, because the random behavior of particles in bed and operator cannot be visually observed. Consequently, there is a strong demand to find effective solutions to tackle these problems.

Relationship Between AE Energy and Flow Pattern in the Bed. In deep fluidized beds, agglomeration formation occurs typically near an elevation from 1/4 to 3/4 of the reactor diameter above the fluidization gas distributor. The bed circulation near the wall changes from generally upward at lower elevations to generally downward at higher elevations, resulting in a "stagnant" zone at this elevation. Hendrickson[28] first pointed out the "stagnant" zone between the two main fluidized circles. Activity of particle motion is minimized in this "stagnant" zone. Also, research by Fujino et al.[29] indicates a stronger tendency for particles to agglomerate in the "stagnant" zone. Thus, it is crucial to detect the fluidization structure- the location of "stagnant" in order to forecast the onset of defluidization.

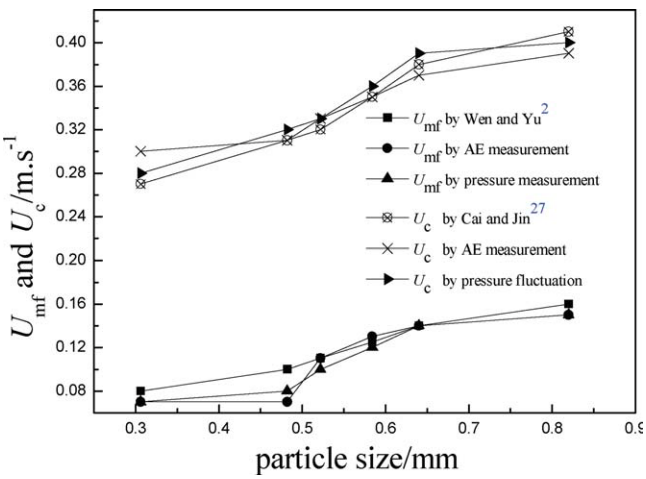

Figure 6. Comparison of U_{mf} and U_c from different methods.

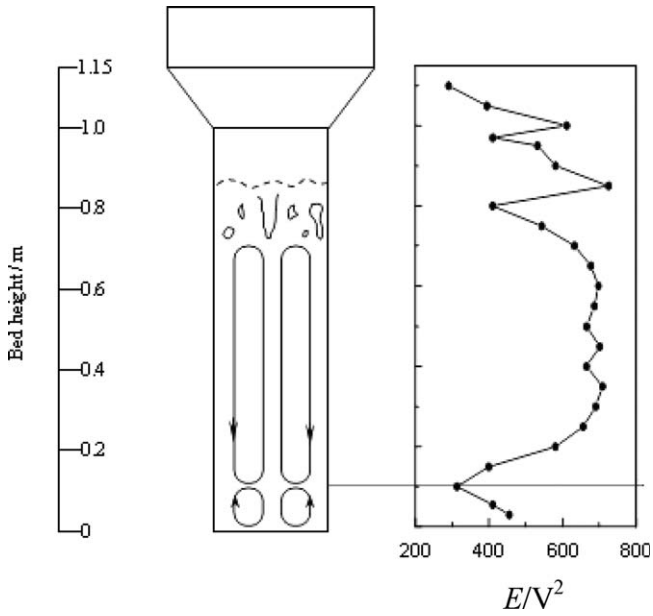

Figure 7. Relationship between AE average energy and bed height (HDPE *d*p = 0.482 mm).

In this instance, the analysis of spatial distribution of AE energy was applied to monitor the activity of particle motion and fluidization status in the gas-solid fluidized bed.

Figure 7 shows the relationship between the AE energy and the bed height when AE sensors are located axially along the wall. There is a "stagnant" zone approximately at the bed height of 0.1–0.2 m, which corresponds to lower amplitude of AE energy for less activity of particles in this region. Typically, agglomeration formation occurs in this zone. Except for the "stagnant" zone, AE energy appears to be higher where fluidization and particle motion are well developed by two particle flow circulations (two main fluidized zone). These two particle flow circulations are formed as a result of the bubbles movement in the bed. Thus, the details about the particle motion activity and the position of "stagnant" zone can be monitored through axially distribution of AE energy. In addition, since unstable fluidization state (agglomeration) often occurs in the position where particles have less activity. Hence, it is feasible to monitor the fluidization state and forecast the emergence of unstable state by AE measurement.

By this way, we obtain the method to estimate the region with particles having relative less activity by analyzing AE spatial energy distribution. However, here comes a problem—what is the threshold of particle activity to occur defluidization, or maybe the relative less activity do not result in the agglomeration?

Theories of Particle Granular Temperature and AE Energy. On the other hand, some granular flow concepts have been employed to reduce the complexity and multiplicity of equations which describe the dynamics of particles, gas, and their interactions. According to the similarity of molecular thermodynamic motion, Campbell[30] proposed the concept of the granular temperature as the "single most important key to understanding the behavior of granular flows". Granular temperature exploits the analogy between the random motion of a dense dusty gas of particles in a fluidized bed and the thermal motion of molecules. However, T^* is not a thermodynamic property, but a steady-state constant determined by the complex interaction between the viscous and inertial forces exerted on a particle by its local gas and particle environment. Often, the conception of granular temperature is quoted to describe the particle motion and activity. Since particle collisions within a fluidized bed are inelastic, the granular temperature can only be a dynamic constant through the power supplied to the bed by the fluidizing gas.

In recent theoretical work on the properties of fluidized beds, there has been an increasing interest toward the granular temperature concept. It gives insights into the study of transport phenomena in such complex systems as, for example, sound propagation, diffusivity and viscosity of dusty gasses, developed from the kinetic theory of dense gasses.[31-34] Unfortunately, despite indications of increasing theoretical interest in the granular temperature concept,[35] there are few reports of the measurement of the granular temperature. Since the concept of granular temperature represents the particle motions, in this article we correlated the AE method and the granular temperature to comprehend the particle motion in the gas-solid fluidized bed.

For n identical particles (with a diameter of d_p, and a mass of m) impact on an area ΔA of the wall of a bed with the normal velocity of v_i, the resultant force $F(t)$ is, thus, given by[36]

$$F(t) = \sum_{i=1}^{n} 2mv_i\delta(t - t_i) \tag{3}$$

where $\delta(t)$ is a Dirac delta function of t, t_i is the arrival time of the ith particle on the wall, and v_i is the vertical velocity of particles impact into the wall for ith particle. Hence, the mean force of particles in unit time can be written as

$$<F(t)> = \frac{\int_0^T F(t)dt}{T} = \frac{2mv\int_0^T \sum_{i=1}^{n} \delta(t - t_i)dt}{T} \tag{4}$$

where v is the mean vertical velocity of particles collide to the wall in the bed. Let f_p denote the average arrival frequency of the particles on the wall, the number of collisions between particles, and the wall in a time interval T is $f_p \cdot T$. So $<F(t)>$ can be described as

$$<F(t)> = 2mvf_p \tag{5}$$

$$f_p = \frac{\rho_F}{m}\Delta Av \tag{6}$$

where ρ_F is the mean density of the fluidized system. For the acoustic pressure P_a can be estimated using $<F(t)>$ and ΔA with the transformation efficiency from the collision pressure to acoustic pressure detected by AE sensor of η

$$P_{AE} = \frac{\eta<F(t)>}{\Delta A} = \frac{2\eta mvf_p}{\Delta A} \tag{7}$$

Thus, acoustic flux J in unit time and acoustic energy E in a time interval T can be expressed as follows

$$\Delta J = P_a \Delta A v = 2\eta m v^2 f_p = 2\eta m v^3 \frac{\rho_F}{m} \Delta A = 2\eta v^3 \rho_F \Delta A \quad (8)$$

$$E = \int_0^T J dt = \int_0^T \int_0^A 2\eta v^3 \rho_F dA dt = 2\eta v^3 \rho_F A T + C_0 \quad (9)$$

where A is the valid receiving area of sensor, and C_0 is the integral constant. It can be seen from Eq. 9 that the AE energy E is a function of transformation efficiency η, fluidized system density ρ_F, particle normal velocity v, and the valid receive area of sensor A. Maintaining the constant operation conditions, such as superficial gas velocity and level of material, both η and A could be considered to be almost constant.

For n identical particles with the same shape, we suppose w_i and E_i as the mass fraction and AE average energy of particle with particle size of di, respectively. E_{mix} is the total AE energy all of the particles. According to the linear superposition principle of AE energy,[37] E_{mix} can be expressed as

$$E_{mix} = \sum_i E_i w_i = 2\eta v^3 \rho_F A t + C_1 \quad (10)$$

C_1 is the integral constant. As shown in Eq. 10, the express of energy for single particle size also fits for the mixed particles. For the fluidized bed, the density of the system can be determined by following equations

$$\rho_F = \frac{H_0}{H_f} \rho_B \quad (11)$$

$$\rho_B = \alpha \rho_p \quad (12)$$

where H_0 and H_f are the fixed-bed height and fluidized-bed height, respectively. ρ_B and ρ_p are the packing density and apparent density of particles, and $\alpha = 1 - \varepsilon_{mf} \approx H_0/H_f$. Batu et al.[38] gave the correlation between H_0 and H_f as

$$\frac{H_f}{H_{mf}} = 1 + \frac{14.311(U_s - U_{mf})^{0.738} d_p^{1.006} \rho_p^{0.376}}{U_{mf}^{0.937} \rho_F^{0.126}} \quad (13)$$

Since $H_{mf} \approx H_0$, so

$$H_f = \left(1 + \frac{14.311(U_s - U_{mf})^{0.738} d_p^{1.006} \rho_p^{0.376}}{U_{mf}^{0.937} \rho_F^{0.126}}\right) H_0 \quad (14)$$

Take, Eqs. 11, 12 and 14 into 10, the total AE energy E_{mix} can finally be written as

$$E_{mix} = \frac{2\alpha\eta v^3 \rho_p A t}{1 + \frac{14.311(u - u_{mf})^{0.738} d_p^{1.006} \rho_p^{0.376}}{u_{mf}^{0.937} \rho_g^{0.126}}} + C_1 \quad (15)$$

For the same settings and conditions, parameters C_1, η and A are constant. Since α is a variable only related to particle property, $\alpha\eta A$ is also constant in this instance.

The granular temperature T^*, is defined as the ensemble average of the squared fluctuation velocity. The value of T^* can be given by $3T^* = \langle w'^2 \rangle = \langle w^2 \rangle - W^2$, where w' is the squared fluctuation velocity, w and W are velocity vector and mean velocity, respectively. For fluidized beds under stable conditions $W^2 \ll \langle w^2 \rangle$ and $W^2 \approx 0$, hence, the mean square of the sphere velocity $\langle w^2 \rangle$, dominates the granular temperature T^*. With the assumptions of spatial uniformity and isotropy, $\langle w^2 \rangle$ can be expressed as $\langle w^2 \rangle = \langle w_x^2 \rangle + \langle w_y^2 \rangle + \langle w_z^2 \rangle = 3\langle w_x^2 \rangle = 3\langle w_y^2 \rangle = 3\langle w_z^2 \rangle$. In that respect T^* can be expressed by one component of $\langle w^2 \rangle$, and the chosen velocity component to be normal to the wall $\langle w_x^2 \rangle$, and, thus, we write $T^* = \langle w^2 \rangle / 3 = \langle w_x^2 \rangle$. According to the definition of w_x, $w_x = v$, T^* can be written as

$$T^* = v^2 \quad (16)$$

Take Eqs. 16 into 15, the relationship between AE energy E_{mix} can be obtained, and the granular temperature T^* in the entire system can be written as Eq. 17

$$T^* = v^2 = \left(\frac{(E_{mix} - C_1)\left(1 + \frac{14.311(U_s - U_{mf})^{0.738} d_p^{1.006} \rho_p^{0.376}}{U_{mf}^{0.937} \rho_g^{0.126}}\right)}{2\alpha\eta A \rho_p t} \right)^{\frac{2}{3}} \quad (17)$$

Miller and Gidaspow[39] pointed out the correlation among the vertical velocity v, superficial velocity U_s, and the particle size d_p for Geldart B particles in the main zone. This has been shown in the following equations

$$v = U_g \left(\frac{D_0}{d_p}\right) \quad (18)$$

where D_0 is the experiential constant, and $D_0 = 0.3$ mm for polyethylene particles.[39] So the granular temperature T^* in the main zone can be written as

$$T^* = v^2 = U_g^2 \left(\frac{D_0}{d_p}\right)^2 \quad (19)$$

Relationship Between E_{mix} and T^* in Different Zone. Experiments have been taken out with particles of different sizes as superficial velocity U_g varied from 0.28 to 0.70 $m \cdot s^{-1}$. Take particle $dp = 0.640$ mm for example, Table 1 shows the correlation between mean energy and superficial velocity in the main and stagnant zone. The value of T^* in

Table 1. Relationship Between Mean Energy and Superficial Velocity in Different Zone ($d_p = 0.640$ mm)

U_g/m·s^{-1}	ω	Mean energy of main zone/V^2	Mean energy of stagnant zone/V^2
0.28	2	110.4	52.2
0.35	2.5	196.3	87.6
0.42	3	383.8	130.2
0.56	4	751.4	328.5
0.70	5	1480.6	675.2

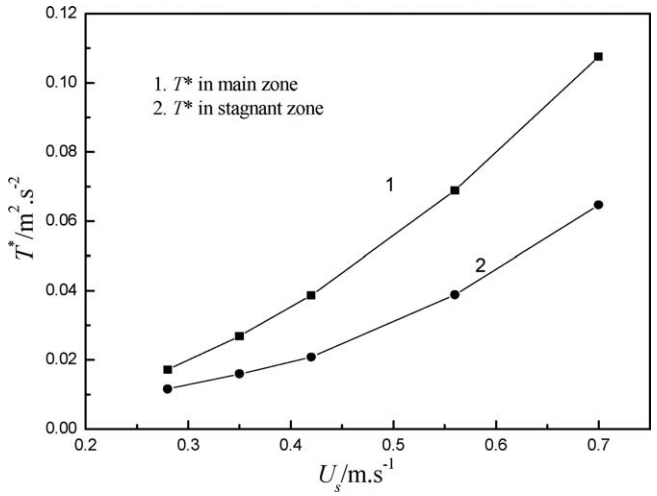

Figure 8. Relationship between granular temperature and superficial velocity in different zones (d_p = 0.640 mm).

main zone is calculated through Eq. 19, and has been shown in Figure 8. In this region, the granular temperature T^* is proportional to the superficial velocity U_g. The cause of the increase in granular temperature was assumed to be the increase in the frequency and strength of particle-particle and/or particle-wall collisions, due to the movement of bed particles as superficial velocity increases.

Take the data of AE mean energy and granular temperature in the main fluidized zone into Eq. 17, the parameters C_1 and $\alpha\eta A$ can be obtained: C_1=−13.4 and $\alpha\eta A$ = 1961.6. Hence, the expression of T^* can be written as

$$T^* = v^2 = \left(\frac{(E_{\mathrm{mix}}+13.378)\left(1+\frac{14.311(u-u_{mf})^{0.738}d_p^{1.006}\rho_p^{0.376}}{u_{mf}^{0.937}\rho_g^{0.126}}\right)}{3923.2\rho_p t} \right)^{\frac{2}{3}} \tag{20}$$

According to Eq. 20, the granular temperature in the "stagnant" zone can be calculated. The results with varied gas velocity have been shown in Figure 8 (the dotted line). As is shown, T^* also increases with U_g in this region, but the values are less than that in main zone under the same gas velocity. This is due to the less particle activity in stagnant zone.

Determination of Particle Motion Activity. Considering the ideal flow pattern without stagnant zone (only main fluidized zone exists), the fluidization state is at its best with no agglomerations when superficial velocity U_s is 3–10 multiples of minimum fluidization velocity U_{mf}.[32,37] That is, the granular temperature in the whole bed should satisfy that $T^* \geq (3\frac{D_0}{d_p}u_{mf})^2$ according to Eq. 19. Due to T^* in stagnant zone is less than that in the main zone, the whole system will be ensured under stable fluidization, and the particles show appropriate activities if the granular temperature in the "stagnant" zone meets that $T^* \geq (3\frac{D_0}{d_p}u_{mf})^2$.

According to the aforementioned analysis, a criterion to guarantee a stable fluidization and appropriate particle motion activity in gas-solid fluidized bed can be obtained based on AE method: The granular temperature in all regions (including main zone and "stagnant" zone) should satisfy that $T^* \geq (3\frac{D_0}{d_p}u_{mf})^2$. Defining the critical granular temperature $T^*_{cr} = (3\frac{D_0}{d_p}u_{mf})^2$, the criterion can be simplified as $T^* \geq T^*_{cr}$. T^*_{cr} is only related to the particle properties.

The Critical Operation Velocity. For particles of d_p = 0.640 mm, the critical granular temperature can be calculated as $T^*_{cr} = (3\frac{D_0}{d_p}u_{mf})^2$ = 0.039 $m^2 \cdot s^{-2}$, and the corresponding superficial velocity is obtained by line two in Figure 8 as U_g = 0.58 $m \cdot s^{-1}$. Beyond the superficial velocity (U_g = 0.58 $m \cdot s^{-1}$), the particles perform appropriate activities, and the whole system is under stable fluidization with no agglomeration in the bed. Although the activity of particles in "stagnant zone" is relatively less, the system still runs stably. To determine the critical point through gas velocity, we define the critical operation velocity U_{cr} as the corresponding superficial velocity to the critical granular temperature T^*_{cr}, which can guide and control the operation in industrial processes.

Effect of Particle Size on T^*_{cr} and U_{cr}. Figures 9 and 10 show the critical granular temperature and critical operation velocity, respectively, for particles with different sizes. As is observed, both the critical granular temperature and critical operation velocity increase with particle size proportionally. The cause is supposed to be the increase of particle powers with particle size, which leads to larger flow rate needed to maintain a good fluidization status.

Determination of Defluidized Zone Above the Distributor. In order to investigate the fluidization details above the distributor for the radial nonuniform distribution of particle movement in the same cross-section, energy analysis was applied based on AE measurement.

In this instance, the fixed-bed height was 20 mm for convenient observation of the fluidization details. AE sensors were mounted under the gas distributor. The measurement of particle distribution above the distributor with the vision system provides a visual indication of the movement of

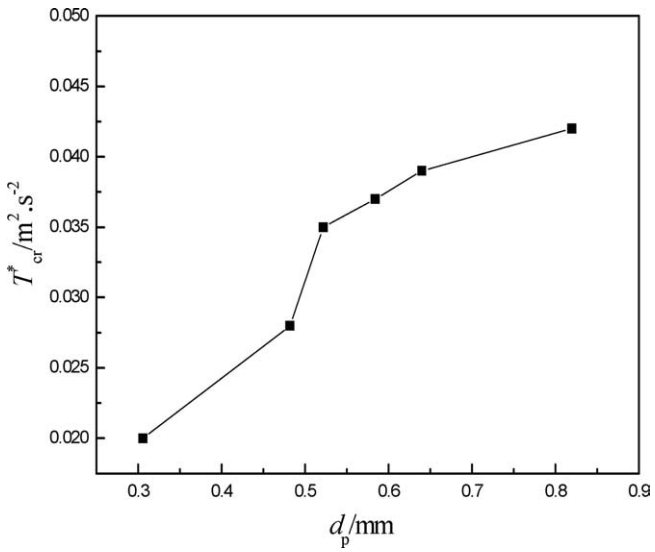

Figure 9. Relationship between T^*_{cr} and d_p.

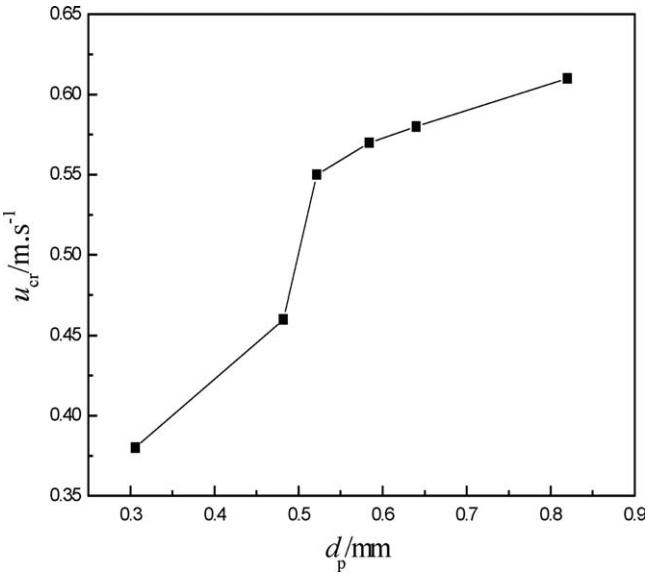

Figure 10. Relationship between U_{cr} and d_p.

particles by photograph device. Thirteen sample points have been arranged and were presented in Figure 11. The average energy of all points have been obtained when the bed fluidized with particles $dp = 0.482$ mm at superficial gas velocity $Ug = 0.65$ m·s^{-1}.

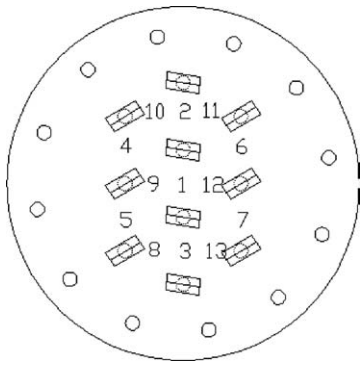

Figure 11. Schematic of distributor.

The result of photograph method has been shown in Figure 12a. In the process of experiments, defluidized regions had appeared above the distributor. This has been illustrated in Figure 12b. The defluidized regions mainly lay in the middle of the distributor, since the structure design is known to play a significant part in influencing the introduction and distribution of the gas stream.[40] From Figure 12c, it can be seen that the distribution of AE energy above the gas distribution and the AE energy amplitude vary remarkably in different sample regions.

Comparing to other points, less amplitude of AE energy appears to occur at point 1, 2 and 3, which are in the regions corresponding to the defluidized zone indicated in

(a) Picture of fluidization

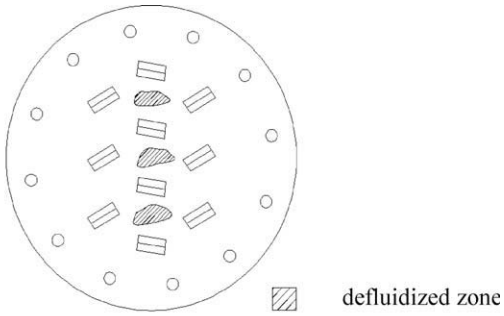

(b) Distribution of defluidized zone

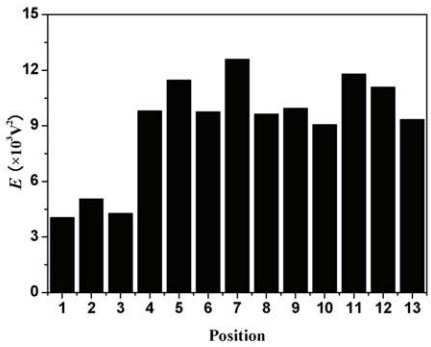

(c) Acoustic energy distribution of measure points

Figure 12. Results comparison between AE method and photograph method: (a) Picture of fluidization; (b) distribution of defluidized zone, and (c) acoustic energy distribution of measure points.

[Color figure can be viewed in the online issue, which is available at www.interscience.wiley.com.]

Table 2. Distribution of Acoustic Energy (U_g = 0.65 m·s^{-1})

Regions	Sample points	E_i/E_{max}
Defluidized zone	1	0.32
	2	0.40
	3	0.34
Fluidized zone	4	0.78
	5	0.91
	6	0.77
	7	1.00
	8	0.77
	9	0.79
	10	0.72
	11	0.94
	12	0.88
	13	0.73

Figure 12b. Hence, different regions can be distinguished by energy analysis as vigorous changes of local particle performance. With the maximum of AE energy E_{max} as a reference, the ratio of the energy of different samples to E_{max}, R_M, was listed in Table 2. It can be found that higher values of R_M were obtained when the measurement points located in fluidized zone. As shown in Table 2, the mean R_M in the defluidized zone is less than 0.4; while in the fluidized zone, it is more than 0.7 by contrast.

Considering the effect of the flow rate, the correlation between the distribution of AE energy and gas velocity was shown in Table 3, with U_g in the range of 0.35–0.55 m·s^{-1}. The results obtained are quite satisfactory. The analysis demonstrates that the distribution tendency with different gas velocities is consistent with that in $Ug = 0.65$ m·s^{-1}, which has been discussed previously. Measurements have been made for particles with different sizes, and the results also show high agreement. Thus, a criterion to detect the defluidized zone above the distributor based on the AE method can be proposed, which is, the defluidized zone exists in the region that the $R_M \leq 0.4$.

Conclusions

In this article, we developed and applied AE technique to real-time monitor, characterize, and control the dynamic transition of flow regimes and particle motion of polyolefin particles in a gas-solid fluidized bed. The AE signals were proved to be *sensitive* and *selective* to the movement of the particles.

Signals from AE sensor located under the gas distributor analyzed by AE temporal energy distribution were proved to be able to indicate the transition of flow regimes. The derivative of AE energy R_E (dE/dv), was proposed and used to obtain the minimum fluidization velocity (the first peak in the curve of R_E vs. U_g), and the onset of turbulent fluidization (the second of peak in the curve of R_E vs. U_g), in good agreement with the classic pressure gradient and fluctuation methods.

Table 3. Distribution of Energy in Different Velocity

U_g/(m·s^{-1})	E_{defmax}/E_{max}	E_{flumin}/E_{max}
0.35	0.35	0.72
0.45	0.39	0.71
0.55	0.38	0.75
0.65	0.40	0.72

In order to control and optimize the fluidization status, the activity of particle motion in different regions was monitored by analyzing AE spatial energy. We proposed to use granular temperature to detect early agglomeration by comparing of granular temperature T^* with T^*_{cr} at the critical condition (i.e., $T^* \geq T^*_{cr}$). The correlation between AE energy and granular temperature showed that highly active particles display high AE energy, leading to high T^*, and, thus, not tending to aggregate ($U_g \geq U_{cr}$). In addition, the definition of critical operation velocity was introduced, which provide significant guides to production in pilot-scale.

Furthermore, experiments were carried out to determine the fluidization details above the gas distributor. AE sensors located under different regions of distributor were able to indicate the distribution of particles above. Then, we presented a criterion to detect the defluidized zone based on the introducing of AE method, which is, defluidized zone exist near the region that the $R_M \leq 0.4$.

Taken together of T^*, R_E, and R_M enables one to identify the fluidization condition system (stable vs. unstable) and particle agglomeration (active vs. inactive).

In this work, the AE technique was proved to be a powerful tool to provide reliable information on the behaviors of particle motion. This methodology showed adequate sensibility and accuracy in the range of experimental conditions analyzed.

Acknowledgments

The authors gratefully acknowledge the support and encouragement of National Natural Science Foundation of China 20490205 and 20736011 and National High Technology Research and Development Program of China (2007AA04Z182).

Notation

A = valid receive area of sensor, m^2
C_0, C_1 C_2 = integral constant
d_p = average particle size, mm
di = average size of particle i, mm
D_0 = experiential constant
E = AE average energy, V^2
E_i = AE energy of particle i, V^2
E_{mix} = AE average energy of particles with different size, V^2
E_{max} = maximum of AE energy, V^2
E_{defmax} = maximum of AE energy in defluidized zone, V^2
E_{flumin} = minimum of AE energy in fluidized zone, V^2
f_p = frequency of particles impact to the wall, s^{-1}
$F(t)$ = force of particles impact to the wall, N
H_0 = fixed-bed height, m
H_f = fluidized-bed height, m
H_{mf} = bed height at U_{mf}, m
m = particle mass, kg
N = points of AE signal serial
J = AE energy flux
P_a = acoustic pressure, Pa
U_c = onset of turbulent fluidization, m·s^{-1}
U_{cr} = critical operation velocity, m·s^{-1}
U_{mf} = minimum fluidization velocity, m·s^{-1}
U_{mb} = minimum bubble velocity, m·s^{-1}
U_g = superficial gas velocity, m·s^{-1}
v = velocity of particles impact into the wall, m·s^{-1}
v_i = velocity of particle i, m·s^{-1}
x_i = sample points of AE signals
t_i = time for the number i particle arrives at the wall, s
T^* = granular temperature, m^2·s^{-2}

T^*_{cr} = critical granular temperature, $m^2 \cdot s^{-2}$
w = velocity vector, $m \cdot s^{-1}$
w_x = velocity vector in x direction, $m \cdot s^{-1}$
w_y = velocity vector in y direction, $m \cdot s^{-1}$
w_z = velocity vector in z direction, $m \cdot s^{-1}$
w_i = mass fraction of particle i, $m \cdot s^{-1}$
w' = squared fluctuation velocity, $m \cdot s^{-1}$
W = mean velocity, $m \cdot s^{-1}$
R_E = derivative of E with respect to superficial gas velocity
R_M = the ratio of the energy of different samples to E_{max}
$\alpha = 1 - \varepsilon_{mf}$
ε_{mf} = void fraction of bed at minimum fluidization velocity
η = transition efficiency
ρ_B = packing density of particles, $kg \cdot m^{-3}$
ρ_F = mean density of the fluidized system, $kg \cdot m^{-3}$
ρ_g = gas density, $kg \cdot m^{-3}$
ρ_p = apparent density of particles, $kg \cdot m^{-3}$
ω = fluidization number
$\delta(t)$ = dirac delta function of t

Literature Cited

1. Davidsion JF, Harrison D. *Fluidized particles*.New York: Cambridge University Press; 1963.
2. Wen CY, Yu YH. A generalized method for predicting the minimum fluidization velocity. *AIChE J*. 1966;12:610–612.
3. Rhodes MJ, Geldart D.Transition to turbulence? *Fluidization V*.New York: Engineering Foundation; 1986: 281–288.
4. Bi HT, Grace JR. Effect of measurement on the velocities used to demarcate the onset of turbulent fluidization. *Chem Eng J Biochem Eng J*. 1995;57(3):261–271.
5. Chen A, Bi HT. Pressure fluctuations and transition from bubbling to turbulent fluidization. *Powder Technol*. 2003;133:237–246.
6. Eills N. Hydrodynamics of gas-solid turbulent fluidized beds. University of British Columbia; 2003. Ph.D. Thesis.
7. Yang TY, Leu LP. Study of transition velocities from bubbling to turbulent fluidization by statistic and wavelet multi-resolution analysis on absolute pressure fluctuations. *Chem Eng Sci*. 2008;63:1950–1970.
8. van Ommen JR, Schouten JC, Coppens MO et al. monitoring fluidization by dynamic pressure analysis. *Chem Eng Technol*. 1999; 22(9):773–775.
9. Scala F, Chirone R. Characterization and early detection of bed agglomeration during the fluidized bed combustion of olive husk. *Energy fuels*. 2006;20(1):120–132.
10. Gajewski A. Investigation of the electrification of polypropylene particles during the fluidization process. *J Electrostat*. 1985;17(3): 289–298.
11. Goode MG, Williams CC, Hussein F D, McNeil T J, Lee K H. Static control in olefin polymerization. US Patent Application 6111034; Aug 29, 2000.
12. Briens,CL, Briens LA, Barthel E et al. Detection of local fluidization characteristics using the V statistic. *Powder Tech*. 1999;102(1): 95–103.
13. Jezl JL, Peters EF. Horizontal reactor for the vapor phase polymerization of monomers. USP4101289,18/07/1978.
14. van Ommen JR, Schouten JC, vander Stappen MLM et al. Response characteristics of probe-transducer systems for pressure measurements in gas-solid fluidized beds: how to prevent pitfalls in dynamic pressure measurements. *Powder Tech*. 1999;106(3):199–218.
15. van Ommen JR, Schouten JC, Coppens MO, Lin W. Timely detection of agglomeration in biomass fired fluidized beds. In: Geiling DW, ed. *Proceedings of the 16th International Conference on Fluidized Bed Combustion 131*. New York: ASME. 2001.
16. Schouten,JC, Bleek,CM. Monitoring the quality of fluidization using the short-term predictability of pressure fluctuations. *AIChE J*. 1998; 44:48–60.
17. Drift A, Visser HJM, Olsen V. Prediction and solution methods for ash agglomeration and related problems during biomass conversion. In: *Proceedings of the First World Conference on Biomass for Energy and Industry*, London, UK; 2001:485–488.
18. Yu ZQ, Chow PS, Reginald BHT. Quantification of particles morphology by boundary Fourier transform and generic Fourier transform. *Chem Eng Sci*. 2007;62(14):3777–3786.
19. Mylvaganam S. Some applications of acoustic emission in particle science and technology. *Part Sci Technol*. 2003;21:293–301.
20. Halstensen M, Esbensen K. New developments in acoustic chemometric prediction of particle size distribution-"the problem is the solution." *J Chemometr*. 2000;14:463–481.
21. Boyd JWR, Varley J. The uses of passive measurement of acoustic emissions from chemical engineering processes. *Chem Eng Sci*. 2001;6(5):1749–1767.
22. Hiroyuki T, Toyokazu Y, Huang CC, Sekiguchi I. Monitoring particle fluidization in a fluidized bed granulator with an acoustic emission sensor. *Powder Tech*. 2000;113:88–96.
23. Cody GD, Bellows RJ, Goldfarb DJ, Wolf HA, Storch Jr GV. A novel non-instrusive probe of particle motion and gas generation in the feed injection zone of the feed riser of a fluidized bed catalytic cracking unit. *Powder Tech*. 2000;110:128–142.
24. Jiang XJ, Wang JD, Jiang BB, Yang YR, Hou LX. Study of power spectrum of acoustic emission (AE) by accelerometers in fluidized beds. *Ind Eng Chem Res*. 2007;46(21):6904–6909.
25. Ren CJ, Jiang XJ, Wang JD, Yang YR, Zhang XH. Determination of critical speed for complete solid suspension using acoustic emission method based on multiscale analysis in stirred tank. *Ind Eng Chem Res*. 2008;47(15):5323–5327.
26. Wang JD, Cao YJ, Jiang XJ, Yang YR. Agglomeration detection by acoustic emission (ae) sensors in fluidized beds. *Ind Eng Chem Res*. 2009;48(7):3466–3473.
27. Cai P, Jin Y, Yu ZQ, Wang ZW. Mechanism of transition from bubble fluidized to turbulent fluidized. *AIChE J*. 1990;36(6):955–956.
28. Hendrickson G. Electrostatics and gas phase fluidized bed polymerization reactor wall sheeting. *Chem Eng Sci*. 2006;61(4):1041–1064.
29. Fujino M, Ogata S, Shinohara H. The electric potential distribution profile in a naturally charged fluidized bed and its effects. *Int Chem Eng*. 1985;25(1):149–159.
30. Campbell C S. Rapid grannular flows. *Annu Rev Fluid Mech*. 1990; 22:57–92.
31. Koch D L. Kinetic theory for a monodisperse gas-solid suspension. *Phys Fluids A*. 1990;2:1711.
32. Gidaspow D.*Multiphase flow and fluidization: continuum and kinetic theory descriptions*.San Diego: Academic Press; 1994.
33. Jenkins JT, Knops RJ, Lacey AA.*Non-classical continuum mechanics*.Cambridge: Cambridge University Press; 1987.
34. Jenkins JT, McTigue DF, Joseph DD, Schaeffer DG.*Two phase flow and waves*.New York: Springer; 1990.
35. Jackson R, Weimer AW. Fluid particle technology. *AIChE Symp Ser*. 1994;90:1–30.
36. Gody GD, Goldfarb DJ, Storch GV, Norris AN. Particle granular temperature in gas fluidized beds. *Powder Tech*. 1996;87:211–232.
37. Haar DT, Band W. Elements of statistical mechanics. *Amer J Phys*. 1954;22(9):641–642.
38. Batu SP, Shah B, Talwalker A. Fluidization correlations for coal gasification materials-minimum fluidization velocity and fluidized bed expansion ratio. *AIChE Symp. Ser*. 1978;74(176):176–186.
39. Miller A, Gidaspow D. Dense, vertical gas-solid flow in a pipe. *AIChE J*. 1992;38(11):1801–1815.
40. Geldart D, Kelsey JR. The influence of the gas distributor on bed expansion, bubble size and bubble frequency in fluidized bed. *I Chem E Symp Ser*. 1968;30:114–125.

Manuscript received Feb. 3, 2009, and revision received July 13, 2009.